



MODELING THE FLEXIBLE NEEDLE INSERTION INTO THE HUMAN LIVER

Veturia CHIROIU, Nicoleta NEDELICU, Ligia MUNTEANU, Cristian RUGINĂ, Marius IONESCU, Ciprian DRAGNE

Institute of Solid Mechanics of the Romanian Academy – Ctin Mille 15, 010141 Bucharest, Romania
Corresponding author: Veturia Chiroiu, E-mail: veturia.chiroiu@imsar.ro

Abstract. We report the deformation of the needle during its insertion into the human liver in the context of surgery simulation of the high- robotic-assisted intraoperative treatment of liver tumors based on the integrated imaging-molecular diagnosis. The bee needle is modeled as a flexible thread within the framework of the nonlinear elasticity theory. The motion equations of the needle are similar to Tzitzeica equations of surfaces which are invariant under the group of centro-affine transformations. That means the surfaces tend to minimize their area and have a minimal Dirichlet energy of how variable a function is. The closed form solutions are obtained for deformation of the needle. In addition, the collision between the needle and the tissues is modeled as a minimization problem.

Key words: bee needle, human liver, nonlinear elasticity theory, Tzitzeica surface.

1. INTRODUCTION

Understanding the surgical needle response during the insertion into the liver is a problem of longstanding interest for the realistic surgical simulators of the cutting procedures for malignant hepatic tumours [1-3]. The treatment of non-resectable hepatic tumors is achieved by delivery into the tumor of an active chemotherapeutic agent with the help of a surgical needle. The needle trajectories are optimized in order to not collide with other organs or tissues, blood vessels or nerves. Fig.1 presents the tumor position and possible collision-free trajectories of the surgical needle.

Current analysis in laparoscopy has stimulated an awareness that the deformations and topological changes of the needle during its passage towards the tumor can have significant effects and repercussions on the surgical act [4]. The needle insertion can cause deformation and even damage of the liver if its deformations are significant [5].

In this paper a surgical robot consisted of a revolute joint and a flexible needle is considered (Fig.1). The Lagrange reference system of coordinates (X, Y, Z) of unit vectors (e_1, e_2, e_3) with the origin O located in the entry point of the skin is attached to the needle. A local Euler system of coordinate with the unit vectors (d_1, d_2, d_3) is attached to the flexible needle to describe the position and orientation of the needle who must carry drugs to the tumor. The angle between the needle and the axis x_1 is $\tilde{\theta}_1$, which represents the generalized coordinate of the rigid system. The serial robot has f degrees of freedom $f = f_r + f_e$, where $f_r = 1$ is the rigid body degree of freedom, and $f_e = 3$ are the elastic degrees of freedom representing the deformations of the needle at bending u_1, u_2 and torsion u_3 . The generalized coordinates vector is $q = [\tilde{\theta}_1, u_1, u_2, u_3]^T$.

The environment containing the organs, ribs, blood vessels and the tumor and possible collision-free trajectories of the surgical needle are represented in Fig.2.

Different types of needles were analyzed before choosing the surgical needle [7, 8]. The flexible bee barbed needle proposed by Sahlabadi [6] is chosen for some of its advantages such as: it decreases the most the insertion force, that is with 24%, and therefore it decreases the tissue deformation by 17% because of the

tip deflection. The characteristics of this needle are: the front angle has 157 deg, the back angle, 110 deg, the height is 0.5mm, and the tip thickness 0.15mm. The honeybee barbed needle model is presented in Fig. 3 [6].

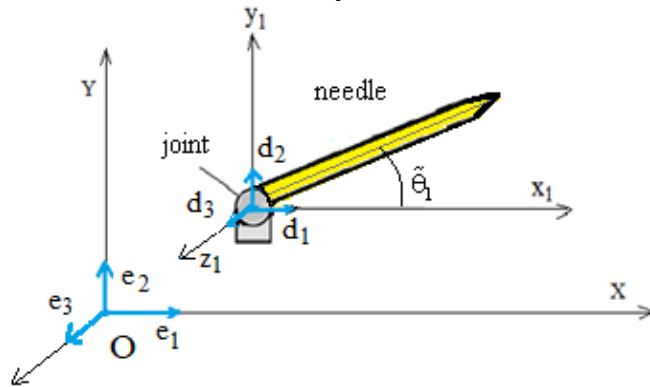


Fig.1 – Surgical robot consisted of a revolute joint and a flexible needle. The Lagrange coordinate system OXY and the local Euler coordinate systems are attached to flexible needle.

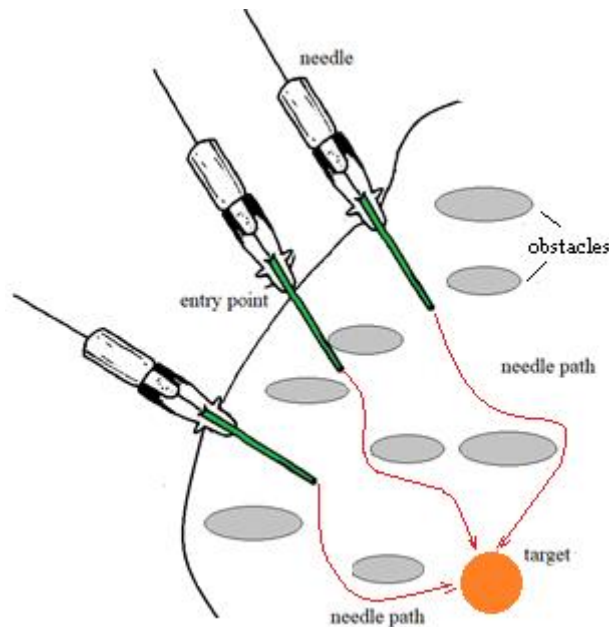


Fig.2 – Tumor position and possible collision-free trajectories of the surgical needle.

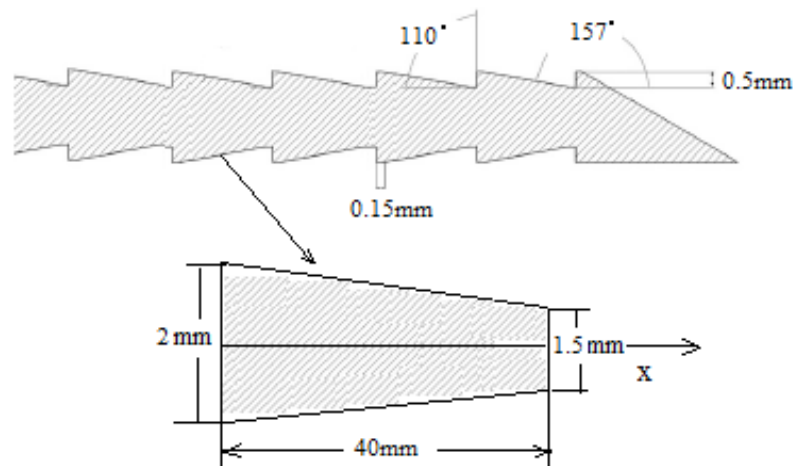


Fig. 3 – Honeybee barbed needle model inspired from [6].

2. MODELING THE FLEXIBLE NEEDLE INSERTION INTO THE HUMAN LIVER

The flexible needle is modeled as an elastic thread within the framework of the elastic theory of the thin elastic thread [9, 10]. The limitation of the current methods existing in the literature consists in applying only 1D linear elasticity theories to a 3D problem with significant nonlinear properties [10, 11].

In what follows, we present some results which fill a gap in the simulation of the surgical needle deformation because, despite the current methods in the modeling of the needle response during its insertion into the tumor, no realistic methods and results have been identified.

Let us consider the case of a tumor located in a difficult place to be reached in the vicinity of the portal tree in the vascular territory of the liver. Location of the tumor, the vascular territory and the vessel branches in the vicinity of the tumor are displayed in Fig.4.

Fig.4a represents location of the tumor and Fig 4b, the vascular territory and the vessel branches in the vicinity of the tumor. It is assumed that the collision-free needle trajectory towards the tumor can take any form even if physically they cannot be realized.

The medical robot is designed for interventions that are difficult to perform in the classic way. In this sense, the restrictions refer to the minimal destruction of healthy tissues (no wrong cuts, no sectioning of blood vessels or nerves). The simplest and most natural shape of the needle trajectory is the straight line which connects the point of entry into the skin to the tumor. But in the most cases, the trajectory can take different forms due to the restriction of avoiding collisions with organs and tissues. Possible such trajectories are displayed in Fig.5, but the optimal shape of the trajectories is obtained from an optimization problem.

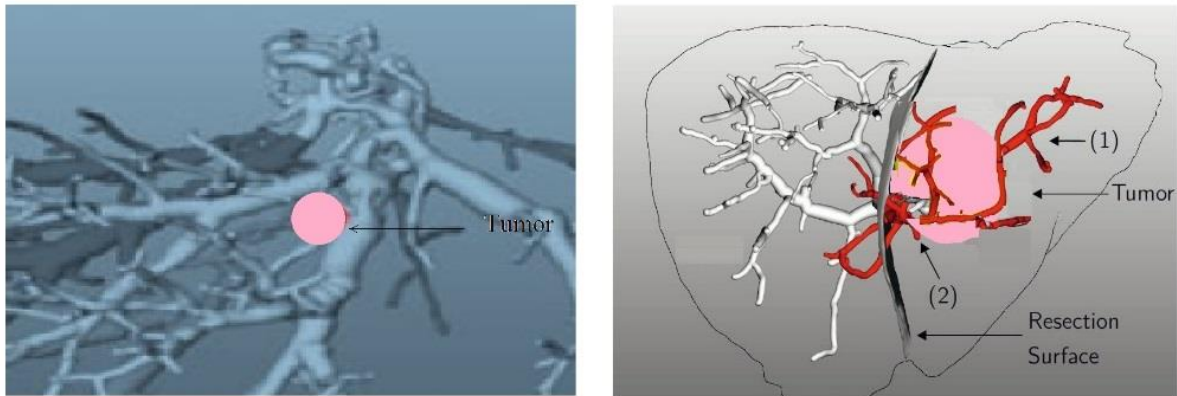


Fig. 4 – a) Location of the tumor; b) Vascular territory (1) and the vessel branches in the vicinity of tumor (2).

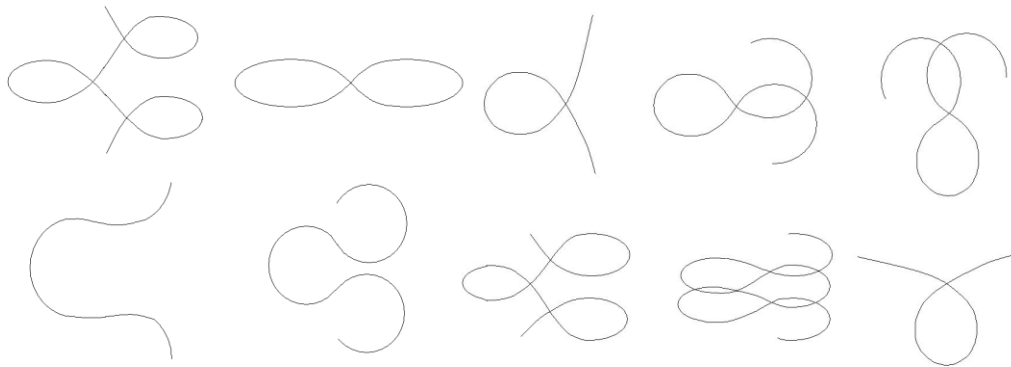


Fig.5 – Different shapes for a trajectory.

The optimization problem of determining the free-collision trajectories of the surgical needle must take into account all difficulties which occur in such operation: (1) the needle must solve its task of transporting drugs into the tumor, (2) the insertion trajectory of the needle should avoid the ribs, blood vessels, and other tissues and organs in the abdominal cavity.

The minimum distance problem can be modeled as a minimization problem that checks the minimum distance between the needle and the tissue [10]

$$\min\left(\frac{1}{2}(r_1 - r_2)^T(r_1 - r_2)\right), \quad (1)$$

with r_1, r_2 the position vectors of two points belonging to the needle and the tissue. The interference distance or penetration is expressed as

$$\min(-d), \quad g_1(r_1) \leq -\frac{d}{2}, \quad g_2(r_2) \leq -\frac{d}{2}, \quad (2)$$

where d is the penetration and g_1, g_2 are the surfaces to the needle and the tissue, respectively (Fig.6).

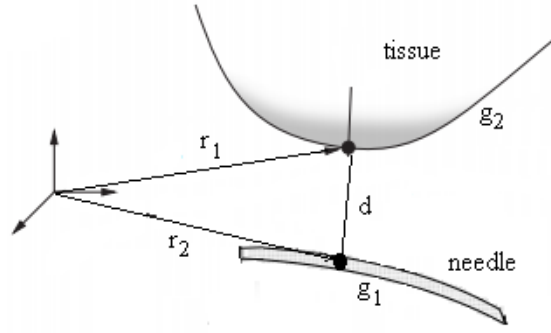


Fig.6 –Minimum distance problem.

Let s be the coordinate along the central line of the natural state of the needle. The simulation is performed for a bee needle made from shape memory alloys with 55% Nickel and 45% titanium, with density $\rho = 6.5 \text{ kg/m}^3$, the modulus of elasticity $E = 32.3 \text{ GPa}$ at bending, and the Poisson's ratio $\nu = 0.48$.

The Lagrange technique is used to obtain the motion equations of the needle with the ends fixed by the force $F = -f$ with $f = (f_1, f_2, f_3)$. This force describes the contact between the needle and the tissue $f = p_c n$. The prime means the partial differentiation with respect to s . The motion equations of the surgical needle are obtained as [9]

$$-\rho \ddot{r} - f' = 0, \quad (3)$$

$$k_1(\dot{\psi}^2 \sin \theta \cos \theta - \ddot{\theta}) - k_2(\dot{\varphi} + \dot{\psi} \cos \theta) \dot{\psi} \sin \theta - A(\psi'^2 \sin \theta \cos \theta - \theta'') + C(\varphi' + \psi' \cos \theta) \psi' \sin \theta - f_1 \cos \theta \cos \psi - f_2 \cos \theta \sin \psi + f_3 \sin \theta = 0, \quad (4)$$

$$-\frac{\partial}{\partial t} \{k_1 \dot{\psi} \sin^2 \theta + k_2 (\dot{\varphi} + \dot{\psi} \cos \theta) \cos \theta\} + \frac{\partial}{\partial s} \{A \psi'^2 \sin^2 \theta + C(\varphi' + \psi' \cos \theta) \cos \theta\} + f_1 \sin \theta \sin \psi - f_2 \sin \theta \cos \psi = 0, \quad (5)$$

$$-k_2 \frac{\partial}{\partial t} (\dot{\varphi} + \dot{\psi} \cos \theta) + C \frac{\partial}{\partial s} (\varphi' + \psi' \cos \theta) = 0. \quad (6)$$

where θ, ψ and φ are the Euler angles, $r(s, t)$ is the position vector which can be interpreted as the image of the central axis in the Euler configuration, $f = (f_1, f_2, f_3)$ is the force applied to the needle, ρ is the mass

density per unit volume, A and C are the bending stiffness and respectively the torsional stiffness of the needle, related to the Lamé constants λ , μ by $A = \frac{1}{4}\pi a^4 E$, $C = \frac{1}{2}\pi a^4 \mu$, where E is the flexural Young's modulus, and a is the radius of the cross section of the needle. The dot means the differentiation with respect to time.

The unknowns in the motion equations (3-6) are the Euler angles θ, ψ and φ . The system of equations (3-6) are solved by the cnoidal method [9]. The method is reducible to a generalization of the Fourier series with the cnoidal functions as the fundamental basis function. This is because the cnoidal functions are much richer than the trigonometric or hyperbolic functions, that is, the modulus m of the cnoidal function, $0 \leq m \leq 1$, can be varied to obtain a sine or cosine function ($m \cong 0$), a Stokes function ($m \cong 0.5$) or a solitonic function, sech or tanh ($m \cong 1$).

The relationship between the Euler angles and the needle deformation is given by

$$\begin{aligned} u_1 &= \theta' \sin \varphi - \psi' \sin \theta \cos \varphi, \\ u_2 &= \theta' \cos \varphi + \psi' \sin \theta \sin \varphi, \\ u_3 &= \varphi' + \psi' \cos \theta. \end{aligned} \quad (7)$$

The functions (u_1, u_2, u_3) measure the bending and torsion of the needle.

3. RESULTS

The minimization problem (1, 2) is solved by using a genetic algorithm [10]. The objective function is minimized

$$\mathfrak{J} = \sum_{i=1}^N \left[\left(\frac{1}{2} (r_{1i} - r_{2i})^T (r_{1i} - r_{2i}) \right) \right]^2, \quad (8)$$

subjected to restrictions

$$\min(-d), \quad g_1(r_1) \leq -\frac{d}{2}, \quad g_2(r_2) \leq -\frac{d}{2}. \quad (9)$$

Three locally 2D optimal collision-free trajectories for the surgical needle corresponding to three different entry points into the skin A, B and C are displayed in Fig.7.

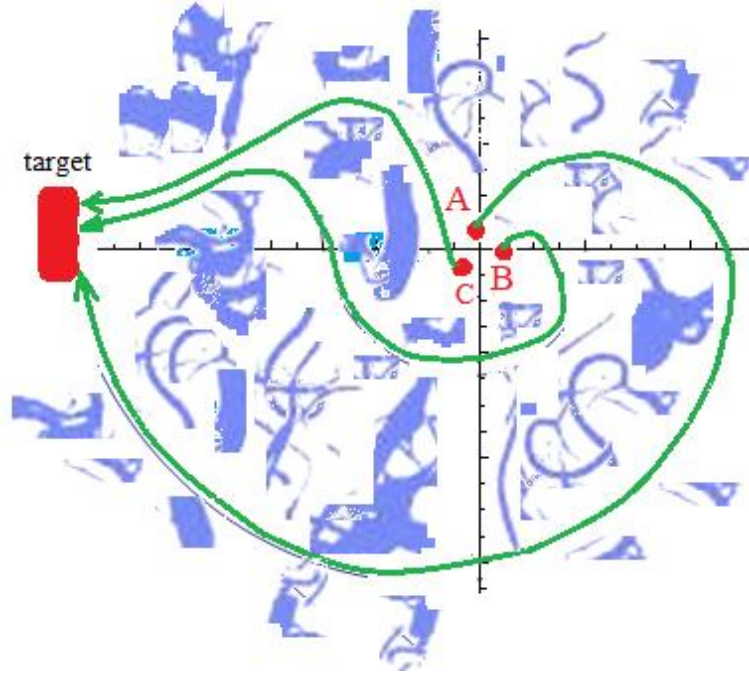


Fig.7 – Three 2D optimal collision-free trajectories for the needle robot.

The motion equations (3-6) possess a special type of solutions. These solutions known as *solitons* are localized functions that conserve their properties even after interaction among them, and then act somewhat like particles [9].

The system of equations has interesting properties: an infinite number of local conserved quantities, an infinite number of exact solutions expressed in terms of the Jacobi elliptic functions (cnoidal solutions) or the hyperbolic functions (soliton solutions), and the simple formulae for nonlinear superposition of explicit solutions.

In addition, these equations are invariants under the group of centro-affine transformations, being similar to the partial differential equations which arise in the Tzitzeica surfaces theory [9]. Tzitzeica surfaces that have the essential property to be invariant under the group of centro-affine transformations [9, 13]. That means that the surfaces locally tend to minimize their area and to have a minimal Dirichlet energy that measures of how variable a function is.

With other words, the surfaces have only local optima, not global optima and the functions are stable with no tendency towards the chaos.

The closed form solutions of the Euler angles θ, ψ and φ are given by [9]

$$\begin{aligned} \cos \theta &= \zeta = \zeta_2 - (\zeta_2 - \zeta_3) \operatorname{cn}^2 \left(\sqrt{\frac{|f_3|}{2A}} (\zeta_1 - \zeta_3) (\xi - \xi_3), m \right) = \\ &= \zeta_2 - (\zeta_2 - \zeta_3) \operatorname{cn}^2 [w(\xi - \xi_3), m], \end{aligned} \quad (10)$$

$$\begin{aligned} \psi &= \frac{1}{4(A - k_1 v^2)^2 w^2} \left\{ -\frac{\beta + (C - k_2 v^2) \tau}{1 - \zeta_3} \Pi \left[w(\xi - \xi_3), \frac{\zeta_2 - \zeta_3}{1 - u_3}, m \right] - \right. \\ &\quad \left. - \frac{\beta - (C - k_2 v^2) \tau}{1 + \zeta_3} \Pi \left[w(\xi - \xi_3), \frac{\zeta_2 - \zeta_3}{1 + u_3}, m \right] \right\}, \end{aligned} \quad (11)$$

$$\begin{aligned} \varphi &= -\frac{\tau [C - A - (k_2 + k_1) v^2]}{A - k_1 v^2} \xi + \frac{1}{4(A - k_1 v^2)^2 w^2} \left\{ \frac{\beta + (C - k_2 v^2) \tau}{1 - \zeta_3} \times \right. \\ &\quad \left. \times \Pi \left[w(\xi - \xi_3), \frac{\zeta_2 - \zeta_3}{1 - \zeta_3}, m \right] - \frac{\beta - (C - k_2 v^2) \tau}{1 + \zeta_3} \Pi \left(w(\xi - \xi_3), \frac{\zeta_2 - \zeta_3}{1 + \zeta_3}, m \right) \right\}, \end{aligned} \quad (12)$$

where $m = \frac{\zeta_2 - \zeta_3}{\zeta_1 - \zeta_3}$ and $w = \sqrt{\frac{|f_3|}{2A}(\zeta_1 - \zeta_3)}$, $\Pi(x, z, m) = \int_0^x \frac{dy}{1 - z \operatorname{sn}^2(y, m)}$ is the normal elliptic integral of the third kind. Functions $\zeta_1, \zeta_2, \zeta_3$ are solutions of the Weierstrass equation

$$\frac{1}{2}\zeta'^2 = a\zeta^3 + b\zeta^2 - a\zeta + c, \quad (13)$$

$$a = -\frac{f_3}{A} \neq 0, \quad b = \frac{1}{2A} \left(\gamma - \frac{C^2 \tau^2}{A} \right), \quad c = -\frac{1}{2A} \left(\gamma - \frac{\beta^2}{A} \right),$$

which admits the soliton solutions [9].

The deformation of the needle during navigation into the liver towards the tumor is represented in Fig. 8. The bending deformation u_1 and u_2 are shown in Fig.8a and the torsion deformation u_3 of the needle in Fig.8b, respectively. While the deformation of the surgical needle has been extensively studied [1-8] many features of the needle behavior remain to be investigated.

Important characteristics of the needle deformation are obtained by intersection of the surfaces u_1, u_2, u_3 with $z = \text{const}$. The 2D hyperbolic manifolds (x, y) with the curvature const/a^4 are obtained. We recognize here the Tzitzeica surfaces which have only local optima not global optima [9, 13]. That means that the deformation of the needle has periodicity properties. These properties derived not only from the properties of the needle but also from the liver properties. Microscopic investigation of the human liver offers details of its microanatomy with emphases to the granular, fibrillar components and irregular solid-fluid interfaces. The mechanical properties of the human liver are investigated in [14] by using a basic functional unit of the liver which comprises a hexagonal and a portal triad -portal vein, hepatic artery, bile duct. The sonification technique for hardly detectable details in the medical images is also applied for the microscopic investigation of the human liver [15]. The 3D manifold of the Tzitzeica variety includes a solid torus and three thickened deformation surfaces, as shown in Fig.9.

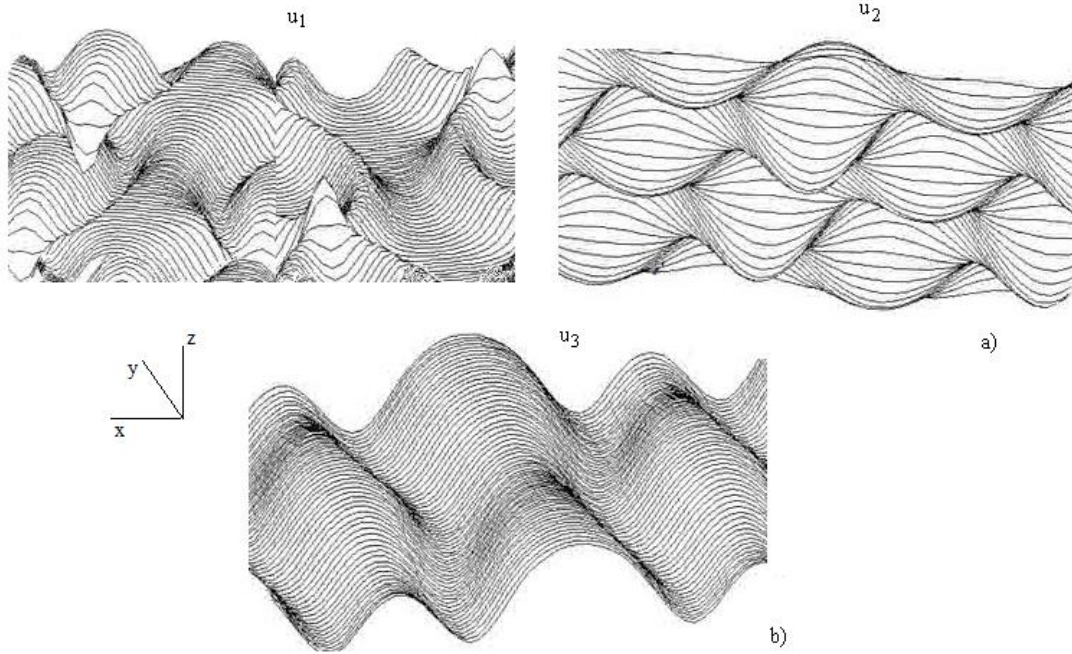


Fig.8 – a) The bending deformation u_1 and u_2 ; b) the torsion deformation u_3 of the needle.

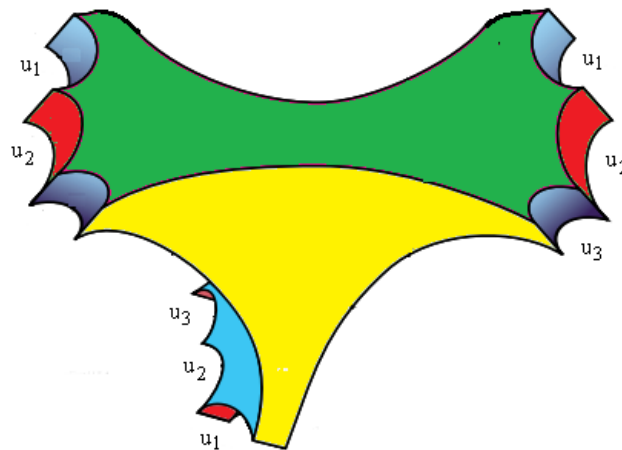


Fig. 9 – The 3D manifold of a Tzitzeica surface.

4. CONCLUSIONS

The surgical bee needle deformation during the insertion into the human liver is considered difficult because of the complexity and variability of the liver. Based on the thin elastic thread theory, the deformation of the bee needle during insertion into the human liver is analyzed.

The motion equations of the needle are similar to equations which arise in the Tzitzeica surfaces and therefore, these equations reveal their invariant properties under the group of centro-affine transformations.

This trend is to minimize the surface area and the Dirichlet energy that measures the stability of the needle deformations. The closed form solutions are obtained for bending and torsion of the needle. The modeling of the collision between the needle and the tissues as a minimization problem that checks the minimum distance between the needle and the tissue is also developed.

ACKNOWLEDGMENTS

This work was supported by a grant of the Romanian Ministry of Research and Innovation, project number PN-III-P1-1.2-PCCDI-2017-0221/ 59 PCCDI/2018 (IMPROVE). Each author has contributed equally for the paper.

REFERENCES

1. J-C LOMBARDO, J-C, M-P CANI, F. NEYRET, *Real time collision detection for virtual surgery*, Computer Animation (CA'99), May 1999, Geneva, Switzerland, pp.82-90, 1999.
2. D. GAO, Y., LEI, B. LIAN, B.YAO, *Modeling and simulation of flexible needle insertion into soft tissue using modified local constraints*, Journal of Manufacturing Science and Engineering, 138, 121012-1-10, 2016.
3. D. PISLA, C., VAIDA, I. BIRLESCU, B., GHERMAN, N. PLITEA, N., *Risk management for the reliability of robotic assisted treatment of non-resectable liver tumors*, Applied sciences, **10**(9), 52, 2020.
4. C. VAIDA, N. PLITEA, N. AL HAJJAR, A. BURZ, F. GRAUR, B. GHERMAN, B., D. PISLA, *A new robotic system for minimally invasive treatment of liver tumours*, Proceedings of the Romanian Academy, series A, Mathematics, Physics, Technical Sciences, Information Science, 2020.
5. F. CALISE, L. CASCIOLA, L. (eds.) *Minimally invasive surgery of the liver*, In collaboration with Ceccarelli, G., Giuliani, A., Patriiti, A., Scuderi, V., ch.30, Giuliante F., Aedito, F., Vellone, M., Nuzzo, G., Segment 4b, Laparoscopic Approach 213-217, Springer 2013.
6. M. SAHLABADI, P. HUTAPEA, *Tissue defomation and insertion force of bee-stinger inspired surgical needles*, Journal of medical device, vol.12, 034501,1-3, 2018.
7. C.K. CHUI, S.H. TEOH, C.J. ONG, *Integrative modeling of liver organ for simulation of flexible needle insertion*, Proceedings of 9th ICARCV, pp. 1-6, 2006.

8. C. SCHUMANN, J. BIEBERSTEIN, C. TRUMM, D. SCHMIDT, P. BRUNERS, M. NIETHAMMER, *Fast automatic path proposal computation for hepatic needle placement*, Proc. SPIE 7625, Medical Imaging 2010: Visualization, Image-Guided Procedures, and Modeling, 76251J, 2010.
9. L. MUNTEANU, St. DONESCU, *Introduction to Soliton Theory: Applications to Mechanics*, Book Series Fundamental Theories of Physics, vol. **143**, Kluwer Academic Publishers, Dordrecht, Boston (Springer Netherlands) 2004.
10. C. BRIȘAN, C. BOANTĂ, V. CHIROIU, *Introduction in optimization of industrial robots. Theory and applications*, Editura Academiei 2019.
11. C. DRAGNE, V. CHIROIU, L. MUNTEANU, C. BRIȘAN, C. RUGINĂ, R. IOAN, N.-D. STĂNESCU, A. STAN, *On the Collision Free-Trajectories of a Multiple-needle Robot based on the Fibonacci Sequence*, New Trends in Mechanism and Machine Science, vol. **89** Mechanisms and Machine Science series, Springer, Chapter 20 pp.1-12, 2019.
12. B. KERBL *et al.*, *Intervention Planning of Hepatocellular Carcinoma Radio-Frequency Ablations*, In Notes in Computer Science 7761, pp. 9-16, Clinical Image-Based Procedures from Planning to Intervention International Workshop, CLIP2012, France, Springer 2013.
13. G. TZITZEICA, *Géométrie projective différentielle des réseaux*, Editura Cultura Natională, Bucharest and Gauthier-Villars, Paris, 1924.
14. V. CHIROIU, N. NEDELICU, D. PISLA, L. MUNTEANU, C. RUGINĂ, *On the mechanical properties of the human liver*, Scientific Reports, 11 (2021) (in press).
15. V. CHIROIU, L., MUNTEANU, R. IOAN, C., DRAGNE, L., MAJERCSIK, *Using the Sonification for Hardly Detectable Details in Medical Images*, Scientific Reports, 9, article number 17711 (2019).

Received , 20